BIOCELL
2023 47(7): 1519-1535

Tech Science Press

A novel prognostic gene signature, nomogram and immune landscape based on tanshinone IIA drug targets for hepatocellular carcinoma: Comprehensive bioinformatics analysis and *in vitro* experiments

Bowen PENG[1]; Yun GE[1]; Gang YIN[2,3,*]

[1] School of Electronic Science and Engineering, Nanjing University, Nanjing, 210023, China
[2] Department of Radiation Oncology, Sichuan Cancer Hospital & Institute, Chengdu, 610041, China
[3] Radiation Oncology Key Laboratory of Sichuan Province, Chengdu, 610041, China

Key words: Tanshinone IIA, Hepatocellular carcinoma, Immune cell infiltration, Prognosis signatures

Abstract: Background: Tanshinone IIA, one of the main ingredients of Danshen, is used to treat hepatocellular carcinoma (HCC). However, potential targets of the molecule in the therapy of HCC are unknown. **Methods:** In this study, we collected the tanshinone IIA targets from public databases for investigation. We screened differentially expressed genes (DEGs) across HCC and normal tissues using mRNA expression profiles from The Cancer Genome Atlas (TCGA). Univariate Cox regression analysis and least absolute shrinkage and selection operator (LASSO) Cox regression models were used to identify and construct the prognostic gene signature. **Results:** Finally, we discovered common genes across tanshinone IIA targets and HCC DEGs. We reported Fatty acid binding protein-6 (FABP6), Polo-like Kinase 1 (PLK1), deoxythymidylate kinase (DTYMK), Uridine Cytidine Kinase 2 (UCK2), Enhancer of Zeste Homolog 2 (EZH2), and Cytochrome P450 2C9 (CYP2C9) as components of a gene signature. The six-gene signature's prognostic ability was evaluated using the Kaplan-Meier curve, time-dependent receiver operating characteristic (ROC), multivariate Cox regression analysis, and the nomogram. The mRNA level and protein expression of UCK2 were experimentally validated after treatment with different concentrations of tanshinone IIA in HEPG2 cells. CIBERSORTx, TIMER2.0, and GEPIA2 tools were employed to explore the relationship between the prognostic signature and immune cell infiltration. **Conclusion:** We established a six-gene signature as a reliable model with significant therapeutic possibility for prognosis and overall survival estimation in HCC patients, which might also benefit medical decision-making for appropriate treatment.

Introduction

Liver cancer ranks sixth in the number of new cases in both sexes. Asia reports the highest numbers in terms of incidence, mortality, and the 5-year prevalence (https://gco.iarc.fr/today/data/). Hepatocellular carcinoma (HCC) represents the most frequent kind of primary cancer, contributing to 90% of the cases (Torre *et al.*, 2015). This incidence is expected to increase in the future, and HCC remains a worldwide health challenge (Llovet *et al.*, 2016; Villanueva, 2019). Chronic liver diseases and fibrosis are the most prominent risk factors for the occurrence of HCC (Balogh *et al.*, 2016), others being viral hepatitis (Choo *et al.*, 1991; Ott *et al.*, 2012), and alcohol consumption (Batey *et al.*, 1992). Non-alcoholic fatty liver disease is emerging as a major reason for HCC in developed countries (Dyson *et al.*, 2014; Kanwal *et al.*, 2016), along with diabetes (Wang *et al.*, 2012; Gao *et al.*, 2013), and obesity (Calle *et al.*, 2003; Reddy and Rao, 2006). It is suggested that obesity elevates the risk of HCC by 1.5 to 4-fold (Larsson and Wolk, 2007). Furthermore, the gender can sometimes influence HCC development, as males are more likely to develop HCC according to studies (Yuan *et al.*, 1995; White *et al.*, 2012). Excessive accumulation of iron status induces a tenfold increase in the likelihood of HCC compared to individuals with regular iron accumulation (Deugnier and Turlin, 2001). Moreover, smoking also was shown be another risk factor in a meta-analysis (Gandini *et al.*, 2008).

*Address correspondence to: Gang Yin, cxqyguestc@163.com
Received: 24 October 2022; Accepted: 15 February 2023;
Published: 23 June 2023

Doi: 10.32604/biocell.2023.027026

Early detection is critical for achieving the best treatment outcome for HCC. Clinically, regenerated nodules arise as a result of hepatocyte proliferation. Ultrasound-detected nodules larger than 1 cm should be followed up with a radiography examination, such as an enhanced phase III or IV computed tomography (CT) or a magnetic resonance imaging (MRI) scan (Sangiovanni *et al.*, 2010; Lee *et al.*, 2015). Furthermore, serum alpha-fetoprotein (AFP) concentrations greater than 400 ng/mL have a substantial positive predictive ability (El-Serag, 2011). Percutaneous biopsies should be confined to nodules that are radiologically nontypical for HCC on CT or MRI (Verslype *et al.*, 2012). Unfortunately, HCC is frequently only detected after patients have developed symptoms and show liver damage and also many individuals are even not thoroughly tested. Several surgical and nonsurgical therapy options are available at the moment for treatment. For example, surgical resection (Allemann *et al.*, 2013), and liver transplantation (Mazzaferro *et al.*, 1996) are suitable treatments for different patients. Other nonsurgical treatments include transarterial chemoembolization (Takayasu *et al.*, 2006), transartetial radiation (Sangro *et al.*, 2011), percutaneous local ablation (Crissien and Frenette, 2014), microwave ablation (Lencioni *et al.*, 2005), and systemic therapy (Llovet *et al.*, 2008; Bertot *et al.*, 2011). Systemic therapies have challenged using conventional therapies for HCC (Bruix *et al.*, 2012). Currently, there is a lot of promise in the molecular profiling-based discovery of new targets and prognostic prediction.

Tanshinone IIA is a representative component of Salvia miltiorrhiza, which has been used to treat cardiovascular diseases. It can reduce pain, enhance blood flow, and stop blood stasis progression (Hao *et al.*, 2018). Pharmacological studies have reported the anti-inflammatory (Yin *et al.*, 2012; Zhao *et al.*, 2016), antioxidant (Gao *et al.*, 2008; Li *et al.*, 2008), and antiangiogenic (Lee *et al.*, 2017) roles of tanshinone IIA. Many studies have also confirmed the newly researched role of tanshinone IIA as an anti-cancer agent (Fang *et al.*, 2021). For example, tanshinone IIA could suppress bladder tumor progression by regulating the STAT3-CCL2 pathway (Huang *et al.*, 2017). Tanshinone IIA could also reduce the growth of pancreatic tumor cells by suppressing the PI3K and MAPK-related signals (Su, 2018). Tanshinone IIA limited tumor growth and cell division by inhibiting the expression of STAT3 in gastric cancer (Zhang *et al.*, 2018). Tanshinone IIA decreased colorectal cancer cell survival through the JNK-Mff signaling pathway (Jieensinue *et al.*, 2018). In another study, tanshinone IIA suppressed the PI3K/Akt signaling pathway, which prevented non-small-cell lung cancer from developing (Liao *et al.*, 2019). Tanshinone IIA inhibited the PI3K/AKT/JNK signaling pathways to cause apoptosis in ovarian cancer cells (Zhang *et al.*, 2019). Additionally, tanshinone IIA restricted glucose metabolism in cervical cancer and promoted apoptosis (Liu *et al.*, 2019b). Tanshinone IIA prevented the expansion of liver cancer by inactivating the transforming growth factor (TGF)-signaling pathway, which is mediated by the SMAD7-YAP connection (Ma *et al.*, 2019). Tanshinone IIA triggered cellular damage in HCC cells by promoting the miR-30b-p53-PTPN11/SHP2 signaling pathway (Ren *et al.*, 2017). Tanshinone IIA is predicted to have multiple targets and multiple pathways in its anticancer potential and function. However, the drug targets and the mechanism of action of Tanshinone IIA that may help improve the prognosis of HCC patients is not yet well understood.

We identified the common gene targets of tanshinone IIA and HCC in this investigation. The risk score of patients was calculated by a 6-gene signature and a nomogram was developed to predict patient survival. Finally, using CIBERSORT, TIMER, and GEPIA2, the correlation of predicted 6-gene signature and immune cell infiltration was investigated. Then, after assessing the possible mechanism, we subsequently confirmed the possible predictive signature of tanshinone IIA. We also validated the effect of tanshinone IIA on UCK2 in HEPG2 cells.

Materials and Methods

Our methodology flowchart is shown in Fig. 1.

Analyzing common genes of tanshinone IIA and HCC

We identified the targets of tanshinone IIA using the TCMSP (Traditional Chinese Medicine Systems Pharmacology Database and Analysis Platform) database (https://old.tcmsp-e.com/tcmsp.php), Swiss target prediction (http://www.swisstargetprediction.ch/), and PharmMapper database (http://www.lilab-ecust.cn/pharmmapper/) by removing the duplicated genes from the three databases. Furthermore, we obtained the differentially expressed genes (DEGs) based on mRNA expression profiling of HCC and paracancerous tissues from the TCGA database. Finally, the overlapping shared genes were the common targets of tanshinone IIA against HCC.

Clinical performance analysis

The clinical characteristics of 362 HCC samples were retrieved from TCGA for subsequent analysis. The information including the survival status, age, gender, the Tumor, Node, Metastasis (TNM) stage, and the ISUP (international society of urologic pathology) grade was provided.

To analyze the overall survival, the Kaplan-Meier (K-M) and time-dependent receiver operating characteristic curve (ROC) curves were examined with R packages “survminer v0.4.6” and “survivalROC v1.0.3”, respectively. The ROC curve’s area under the curve (AUC) is the most essential parameter. The AUC cut-off value was close to 0.5. The closer the value was to 1, the better the diagnostic capabilities.

Development of the prognosis signature

We first separated the 362 HCC samples into training and validation cohorts. Univariate COX regression analysis was performed by R-package “survival v3.1-8”. LASSO analysis was conducted using the R package “glmnet v4.1-4” to further optimize the results. Then, a six-gene signature was proposed from the results of the LASSO analysis. The risk score (RS) was expressed as: $RS = \sum_{i=1}^{n} \beta_i \times Exp_i$, in which βi is the coefficient of gene i, Expi indicates the expression of gene i. Then, patients were split into high- and low-risk

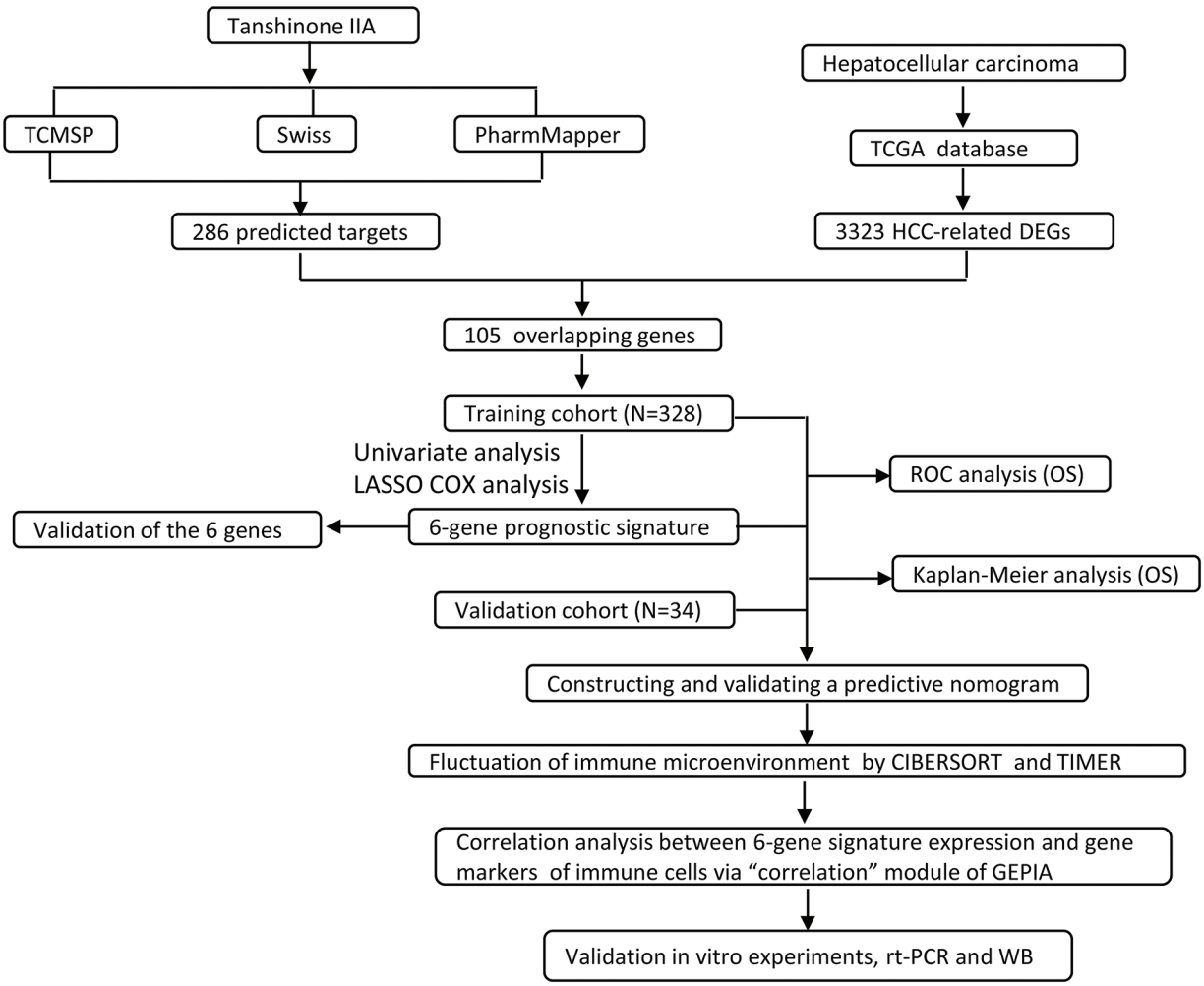

FIGURE 1. The overall flow chart of this study.

categories according to the RS. To evaluate the predictive performance of the risk score, K-M, and time-dependent ROC curve analyses were carried out in both cohorts.

The patient's risk score and several clinical factors were incorporated in univariate and multivariate COX regression analysis. Then, the factors meeting $p < 0.05$ in both COX analyses were used to create a nomogram with R package "rms v5.1-4" to predict patient survival.

Immune cell infiltration analysis

CIBERSORTx (https://cibersortx.stanford.edu/) is a machine learning tool that estimates gene expression profiles and the number of cell types among mixed cellular components using gene expression data (Newman *et al.*, 2019; Steen *et al.*, 2020). CIBERSORTx is a support vector machine (SVM) framework-based deconvolution algorithm, namely a linear combination of the expression level of the gene in different cell subpopulations and the weight of cell fractions in the sample. The algorithm is superior in identifying and estimating the abundance of immune cells. The approach provided a LM22 gene signature matrix file that can specifically discriminate 22 immune cell types by uploading the gene expression file of 362 HCC samples. We next assessed the percentage of 22 immune cells of the high- and low-risk groups with the Wilcoxon test.

TIMER2.0 (http://timer.cistrome.org/) is another comprehensive online tool for analyzing and visualizing immune infiltrates in the TCGA database. TIMER2.0 quantified 6 immune cells, including CD4+ T cells, CD8+ T cells, B cells, neutrophils, macrophages, and dendritic cells. The results of the CIBERSORTx analysis revealed that the overall fraction of the 22 immune cells combined was 100%. Unlike CIBERSORTx, TIMER2.0 did not normalize the predicted value to 1. Hence, the result could not be understood as cell proportion or compared across data sets. We investigated the relationship between the prognostic signatures and six immune infiltrates.

Additionally, the "Correlation Analysis" of the Gene Expression Profiling Interactive Analysis (GEPIA), in this work, GEPIA2 (http://gepia2.cancer-pku.cn/#correlation) was employed to assess the relationship of the suggested signatures of nine immune-related T cells with the prognostic signatures.

Validation of the expression of the prognostic signatures

We then acquired the expressions of prognostic signatures from UALCAN (http://ualcan.path.uab.edu) to further evaluate the prognostic signatures. The expression of the six genes was verified based on sample types and individual cancer stages.

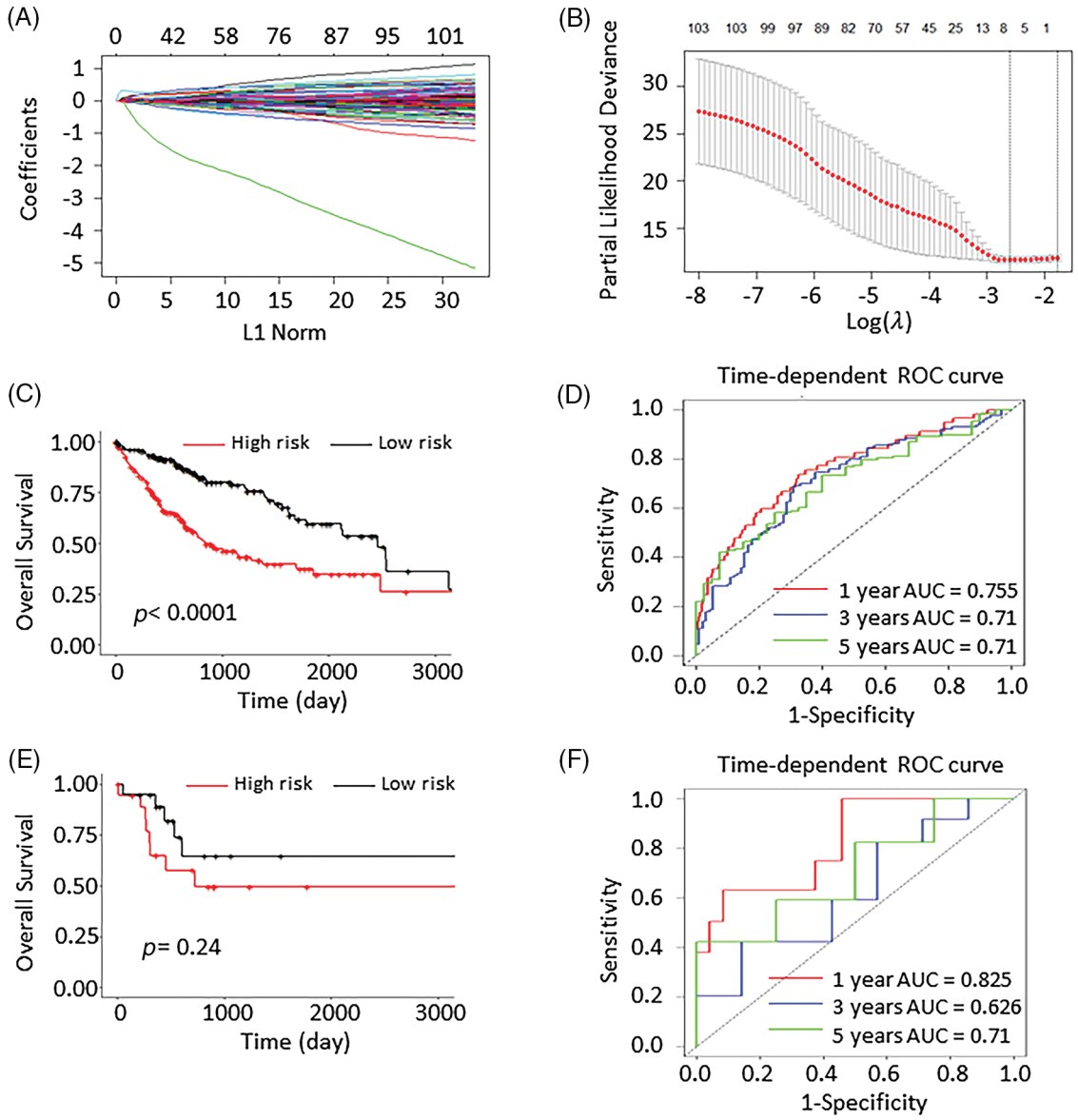

FIGURE 2. Least absolute shrinkage and selection operator (LASSO) analysis and the validation of the 6-gene prognostic signature. (A) The coefficients of 105 genes in LASSO analysis. (B) LASSO coefficients distribution deviation with partial likelihood. (C) The Kaplan Meier (K–M) curves of the high- and low-risk group scores predictions in the training group. (D) The 1-, 3-, and 5-year ROC curves in the training group. (E) The K-M curve of high- and low-risk group scores predictions in the validation group. (F) The 1-, 3-, and 5-year ROC curves in the validation cohort.

Reverse transcription Polymerase Chain Reaction (PCR) assay

The effect of tanshinone IIA on HEPG2 cells was validated using the UCK2 gene. HEPG2 cells (Shanghai EK-Bioscience Biotechnology Co., Ltd., Shanghai, China) in each group were collected after 48 h without/with tanshinone IIA (Merck, Ltd., Chengdu, China) treatment, namely control group, 50 and 100 μM tanshinone IIA groups. The TRIzol solution (Thermo Fisher Scientific, Waltham, USA) was employed to obtain total RNA from cells. The RNA purity and concentration were assessed using an ultraviolet spectrophotometer (Shimadzu UV-3600i Plus). Subsequent to reverse transcription of the UCK2 mRNA to cDNA, which was utilized as a template and replicated in the real-time Polymerase Chain Reaction (RT-PCR) system. The detailed procedure can be found in the previous research for reference (Nolan *et al.*, 2006; Green and Sambrook, 2018). The relative mRNA level of UCK2 was measured with β-actin provided as an internal reference.

Western blotting assay

The cells of all groups were treated with RIPA reagent (Thermo Fisher Scientific, Waltham, USA) for 30 min before being moved to the tube. The supernatant was removed after 10 min of centrifugation at 12,000 r/min. After sodium dodecyl-sulfate polyacrylamide gel electrophoresis (SDS-PAGE) separation, protein bands on the gel were transferred to a polyvinylidene difluoride (PVDF) membrane (Thermo Fisher Scientific, Waltham, USA) and then the membrane was coated with 5% nonfat milk for 1 h at room temperature. Anti-UCK2 antibodies

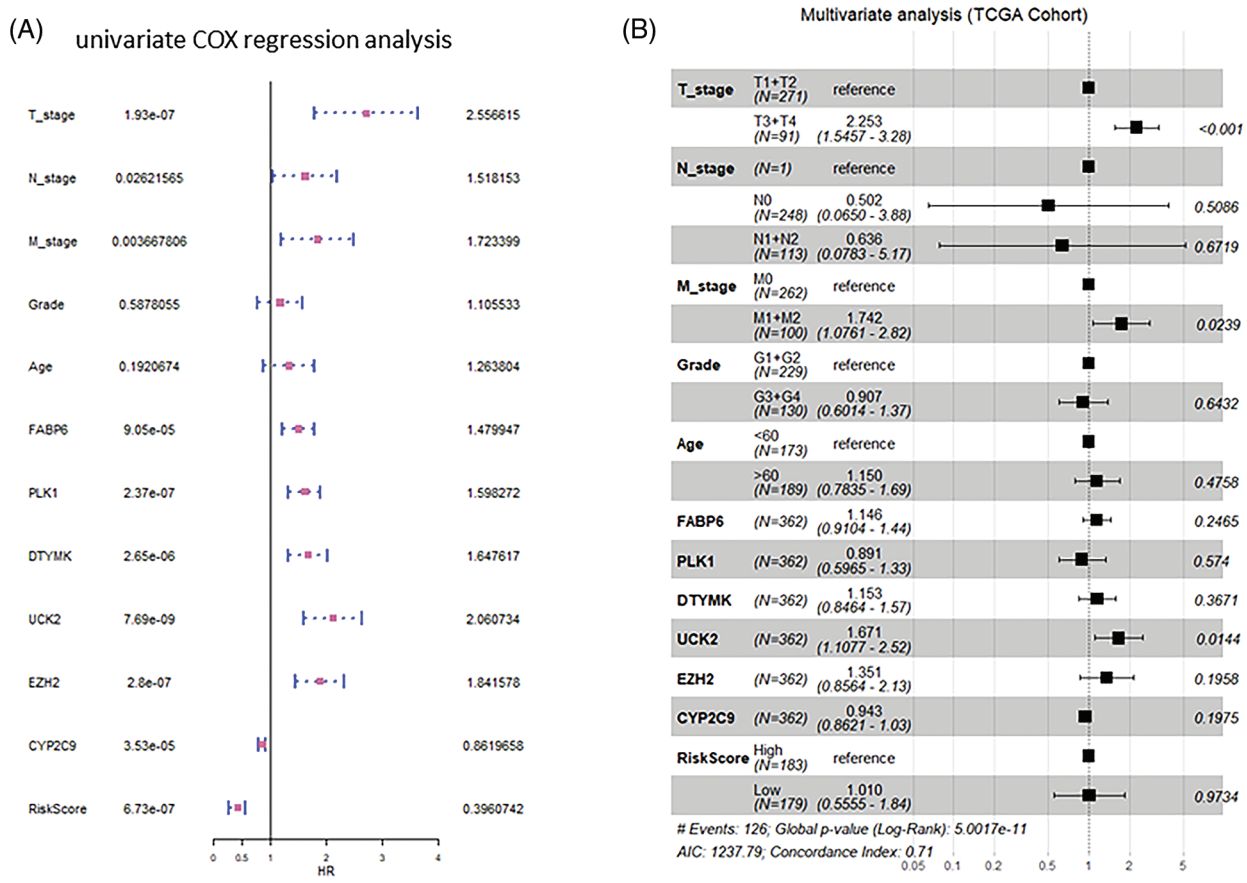

FIGURE 3. Forest graphs of univariate and multivariate Cox analysis. (A) Forest graphs depicting the findings of the univariate Cox regression analysis. (B) Forest plots displaying the results of the multivariate Cox regression analysis.

(Abcam, Cambridge, UK) (ab167683, 1:1000) were added and incubated overnight at 4°C. This was followed by incubation with goat anti-mouse IgG HRP (Abcam, Cambridge, UK) (ab205719, 1:1000) and then stained with the ECL kit (Thermo Fisher Scientific, Waltham, USA). The Gel Imaging System was employed to examine the gray level. The relative expression of each protein band was analyzed to tubulin, which served as an internal control.

Statistical analysis

The R packages were conducted in R 4.1.3. The statistical data of real-time RT-PCR and western blotting were shown as mean ± standard deviation (SD). The data were analyzed and shown by GraphPad Prism 6 with the two tailed-student *t*-test. Statistical significance was defined at $p < 0.05$.

Results

Overlapping genes between tanshinone IIA and hepatocellular carcinoma

The TCMSP showed that the OB (oral bioavailability) value was 49.89% (OB > 30%), and the DL (drug likeness) value was 0.40 (DL > 0.18), which meant that tanshinone IIA has a high absorbance and superior druggability. We searched tanshinone IIA targets in TCMSP, Swiss target prediction and PharmMapper databases. We found 38, 43, and 219 targets in each database, respectively. By deleting the duplicated genes from the three databases, we ultimately came up with 286 targets (Suppl. Table S1). Then, we found 3323 DEGs between the healthy cells and the HCC tissues and 105 genes shared by the DEGs of HCC, and the targets of tanshinone IIA.

Risk prognosis signature and nomogram development

The training cohort (n = 328) and validation cohort (n = 34) were selected at random from the 362 HCC patients. Univariate COX regression analysis was performed and we identified 26 genes that were substantially associated with the overall survival. LASSO COX analysis was employed to understand the outcomes even further. Consequently, we discovered 6 genes (FABP6, PLK1, DTYMK, UCK2, EZH2, and CYP2C9) that were highly significant for patient survival prediction (Figs. 2A and 2B). LASSO COX analysis findings were used to develop a 6-gene signature. The formula used was RS = 0.0057 × FABP6 + 0.0043 × PLK1 + 0.0501 × DTYMK + 0.3090 × UCK2 + 0.0795 × EZH2 − 0.0296 × CYP2C9. Hence, each individual had a risk score computed.

By computing the risk score, 328 patients in the training cohort were separated into 168 low-risk and 160 high-risk patients. In the validation cohort, the 34 patients were grouped into 11 low-risk and 23 high-risk individuals. Compared to the high-risk group, the low-risk had

dramatically improved patients survival ($p < 0.0001$; Fig. 2C). The AUCs at 1-, 3-, and 5-years were 0.755, 0.71, and 0.71, respectively. This demonstrated that the risk prognosis signature has a significant prognostic value in the training cohort (Fig. 2D). The K-M curve analysis of the validation cohort ($p = 0.24$; Fig. 2E) validated these preceding findings. The AUCs of the 1-, 3-, and 5-year survival were 0.825, 0.626, and 0.71, respectively (Fig. 2F).

To verify the credibility of the model, the mean AUC values of the ROC curve were validated using a 5-fold validation (Suppl. Fig. S1). The GEO dataset GSE76427 was additionally searched for validation, and K-M curves and 1, 3, and 5-year AUC curves were plotted to validate the risk model, as shown in Suppl. Fig. S2.

The findings of univariate and multivariate COX regression analyses showed that the TNM stage and the risk score had a substantial connection with overall survival in both training and validation groups (Fig. 3). Subsequently, both these factors were included in the development of the nomogram. The prediction ability of the nomogram created by combining the TNM stage and risk score (C-index = 0.691; Fig. 4A) was superior to the only the risk score (C-index = 0.672) or TNM stage (C-index = 0.564). Furthermore, the results of validation cohorts indicated an almost matching prediction performance with the training cohort (Fig. 4B).

The immune cell infiltration status

The SVM-based CIBERSORTX method was used to calculate the abundance of immune cells infiltration in 362 patients. The abundance of 22 immune cells was shown in 362 distinct tumor samples (Fig. 5A). The overall infiltration percentages of these 22 immune cells was then demonstrated (Fig. 5B). Of these, T cells and macrophages had the largest infiltration ratio. As shown in Fig. 5B, the CD4 naive T cells (26.6506%), plasma cells (14.6888%), follicular helper T cells (Tfh; 7.3556%), M1 macrophages (6.4843%), and M2 macrophages (5.9386%) occupied the larger proportion in the tumor microenvironment. CD4 memory resting T cells ($p = 0.021$), resting NK cells ($p = 0.034$), and activated mast cells ($p = 0.045$) showed significant variations in high- and low-risk individuals (Fig. 6).

To further demonstrate innate gene regulation, we used TIMER2.0 to obtain prognostic signature-mediated changes in the immune cell infiltration profile. The infiltration of six immune cells (CD8+ T cells, CD4+ T cells, B cells, neutrophils, dendritic cells, and macrophages) was shown to

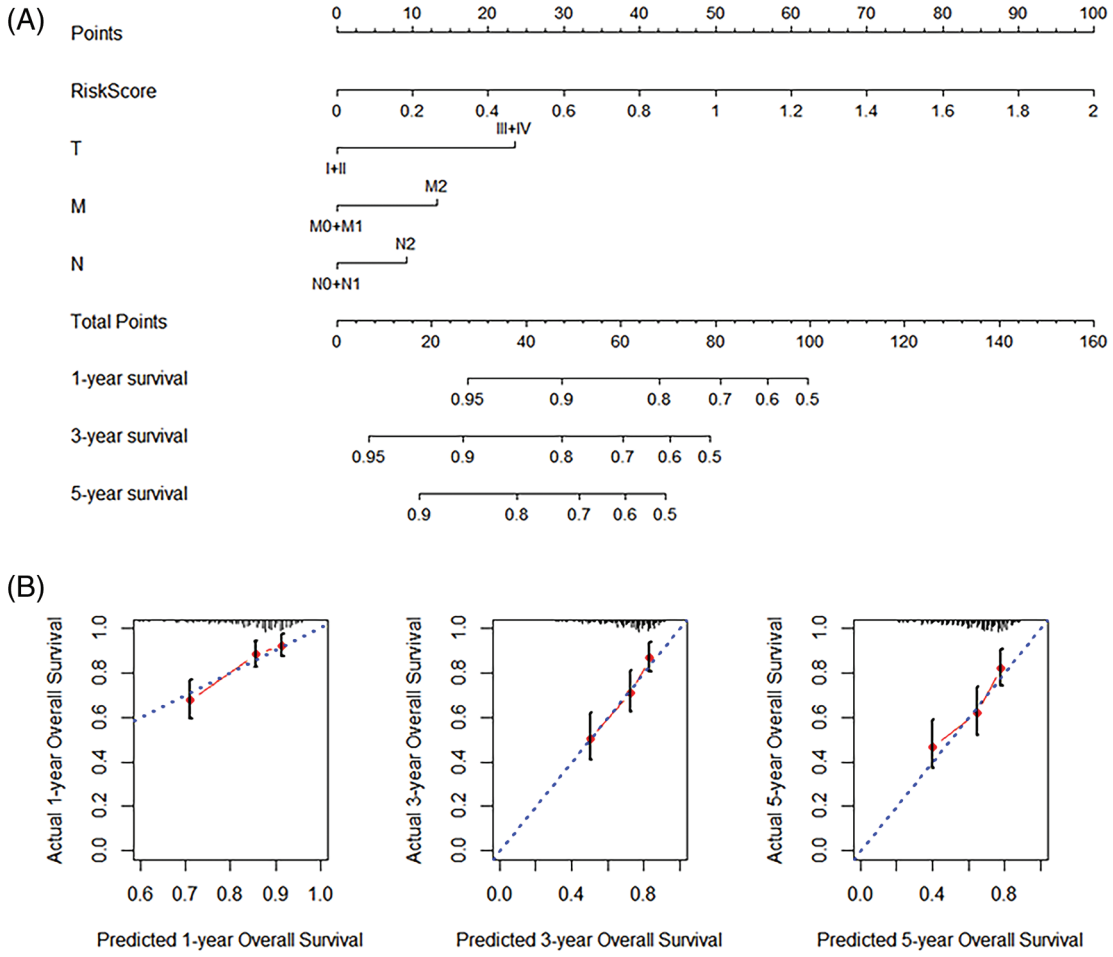

FIGURE 4. Nomogram development. (A) Nomogram with the combined (Tumor, Node, and Metastasis) TNM stage and the risk score. (B) The validation calibration curve of the nomogram for 1-, 3-, and 5-year survival, separately.

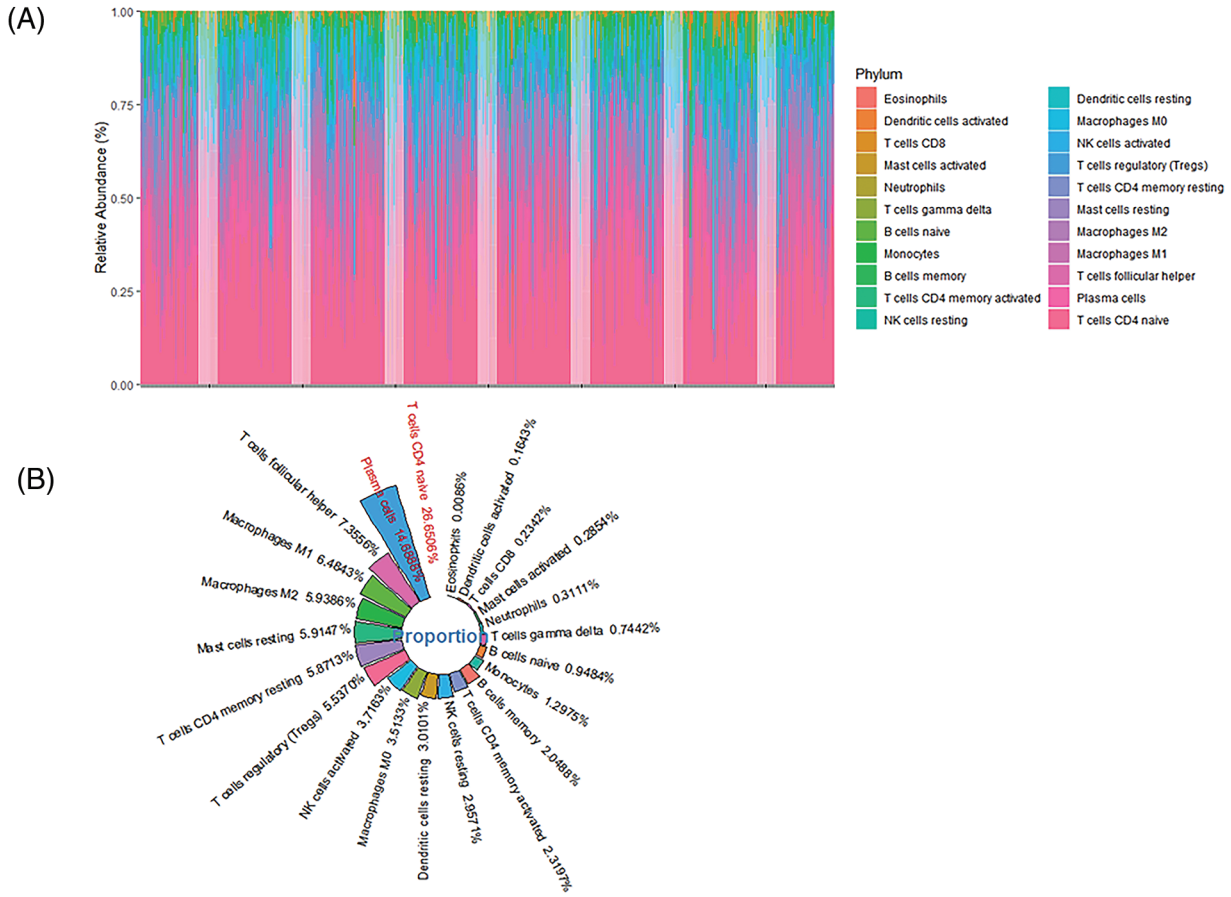

FIGURE 5. The infiltration ratio of 22 immune cells found in patients. (A) The abundance of immune cell (22 cell types) infiltration in 362 hepatocellular carcinoma (HCC) patients. (B) The mean infiltration ratios of 22 immune cell types in 362 HCC samples were then ranked.

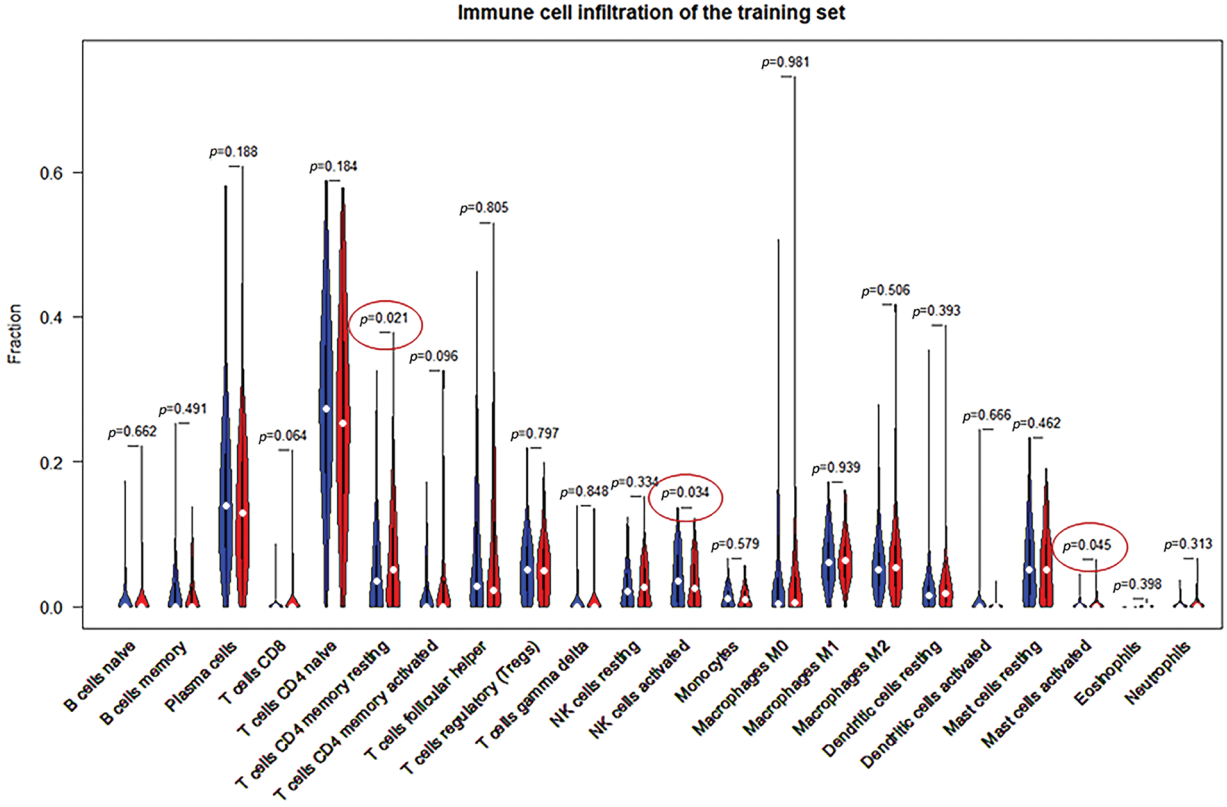

FIGURE 6. Comparison of the 22 immune cell types and their infiltration in high- and low-risk samples.

be substantially linked with the expression of the 6 prognostic signature genes (FABP6, PLK1, DTYMK, UCK2, EZH2, and CYP2C9) (Fig. 7). The high expression of FABP6, PLK1, DTYMK, UCK2, and EZH2 considerably increased the extent of infiltration of the six immune cells. On the contrary, a high expression of CYP2C9 significantly lowered the degree of infiltration (Fig. 7).

For "correlation analysis" in GEPIA2, we computed the correlation between the 6-gene signature (FABP6, PLK1, DTYMK, UCK2, EZH2, and CYP2C9) and the suggested gene set of each immune cell.

Validation of the six-gene signature

To confirm the importance of the gene signature based on FABP6, PLK1, DTYMK, UCK2, EZH2, and CYP2C9, we probed the mRNA expression based on sample types and individual cancer stages by UALCAN. The expression of FABP6, PLK1, DTYMK, UCK2, and EZH2 was increased in the primary tumor compared with the normal tissues, while the expression of CYP2C9 was decreased in the primary tumor group (Fig. 8). The expression of the 6 genes documented a similar trend in the individual cancer stages (Fig. 9).

Effect of Tanshinone IIA on UCK2 mRNA and protein expression levels in HEPG2 cells

As the *p*-value of the UCK2 gene was 0.0144 in the Cox model, which was the most significant it was considered to be the best choice for validation. Further, UCK2 plays a crucial role in liver cancer progression and represents a potential target for developing novel therapies. UCK2 has also been shown to promote cell proliferation, survival, invasion, and angiogenesis (Fu *et al.*, 2022), leading to a more aggressive phenotype of cancer cells. Moreover, UCK2 has been shown

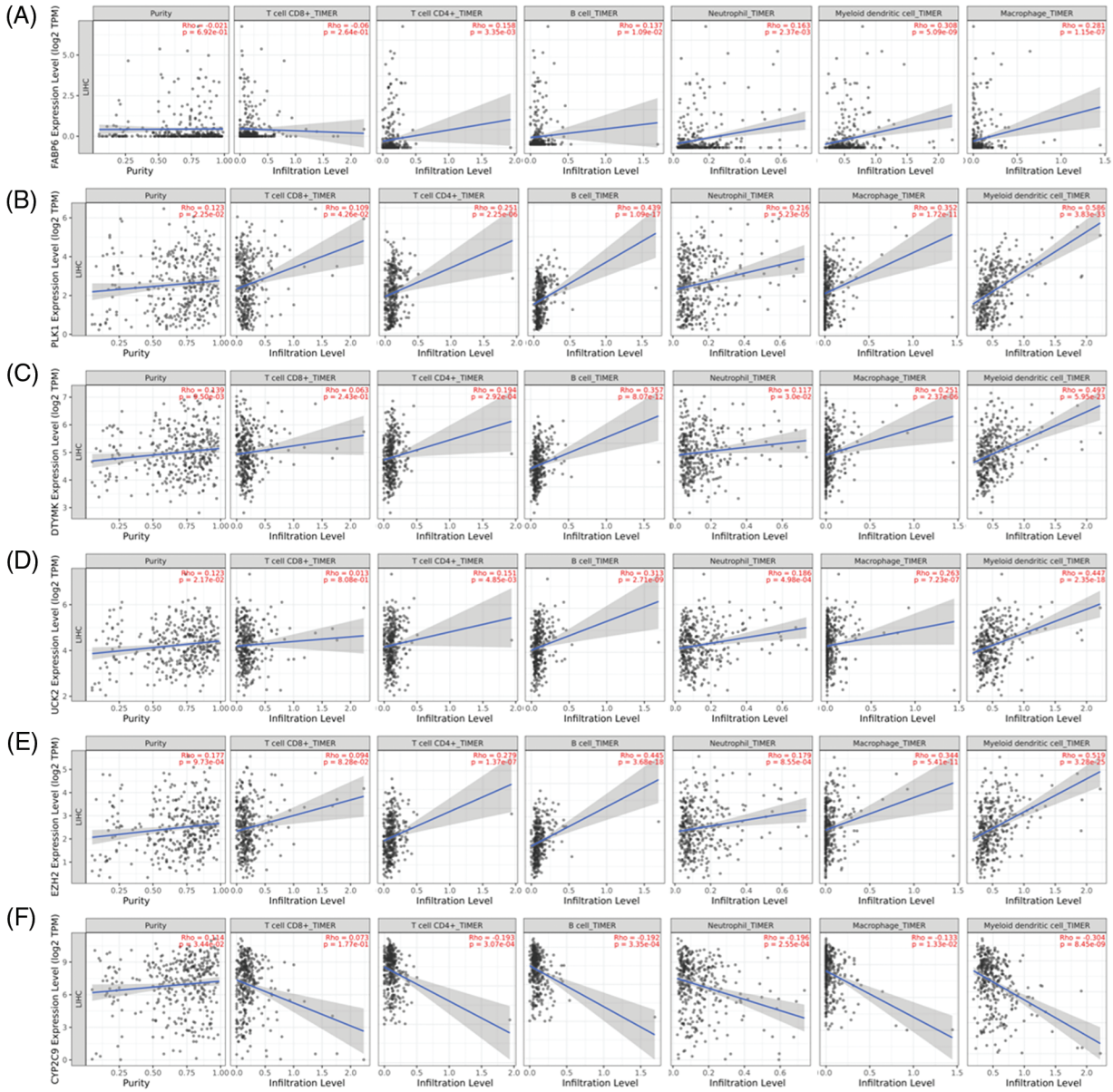

FIGURE 7. Correlation of the expression of six prognostic genes and the infiltration of six immune cells from the TIMER2.0 collection. (A) FABP6; (B) PLK1; (C) DTYMK; (D) UCK2; (E) EZH2 and (F) CYP2C9.

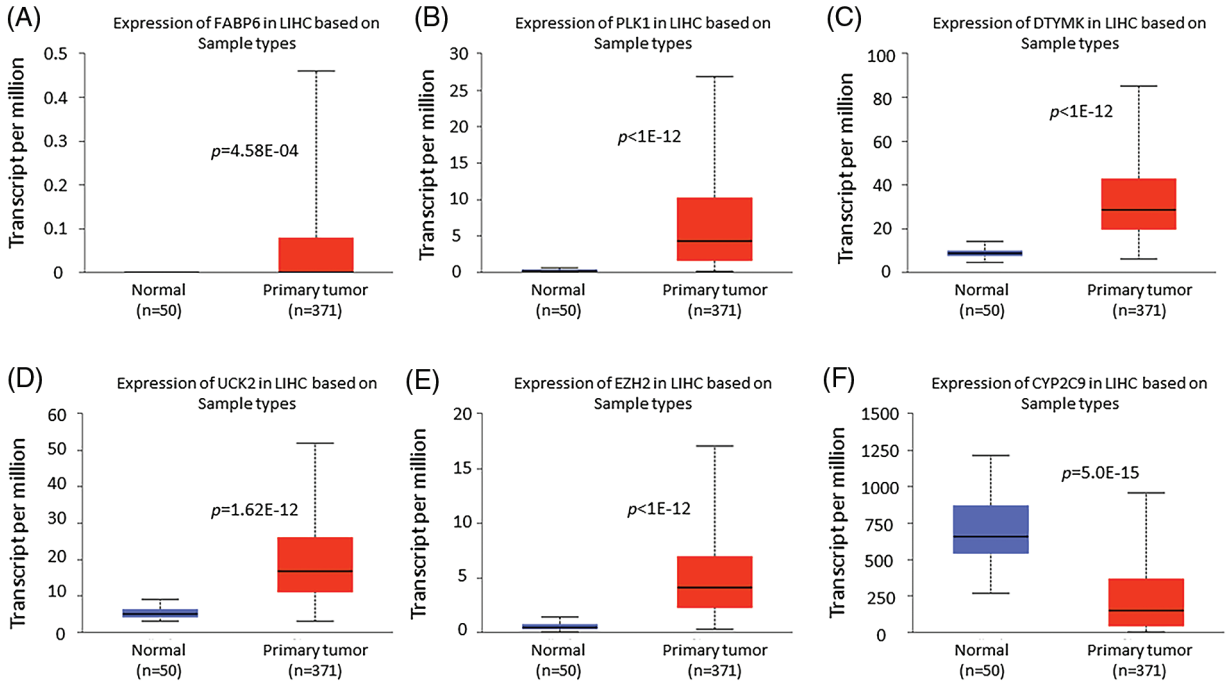

FIGURE 8. Box plots of the 6 prognostic gene expression obtained using UALCAN. Differential expression of FABP6 (A), PLK1 (B), DTYMK (C), UCK2 (D), EZH2 (E), and CYP2C9 (F) in normal tissues *vs.* primary tumors.

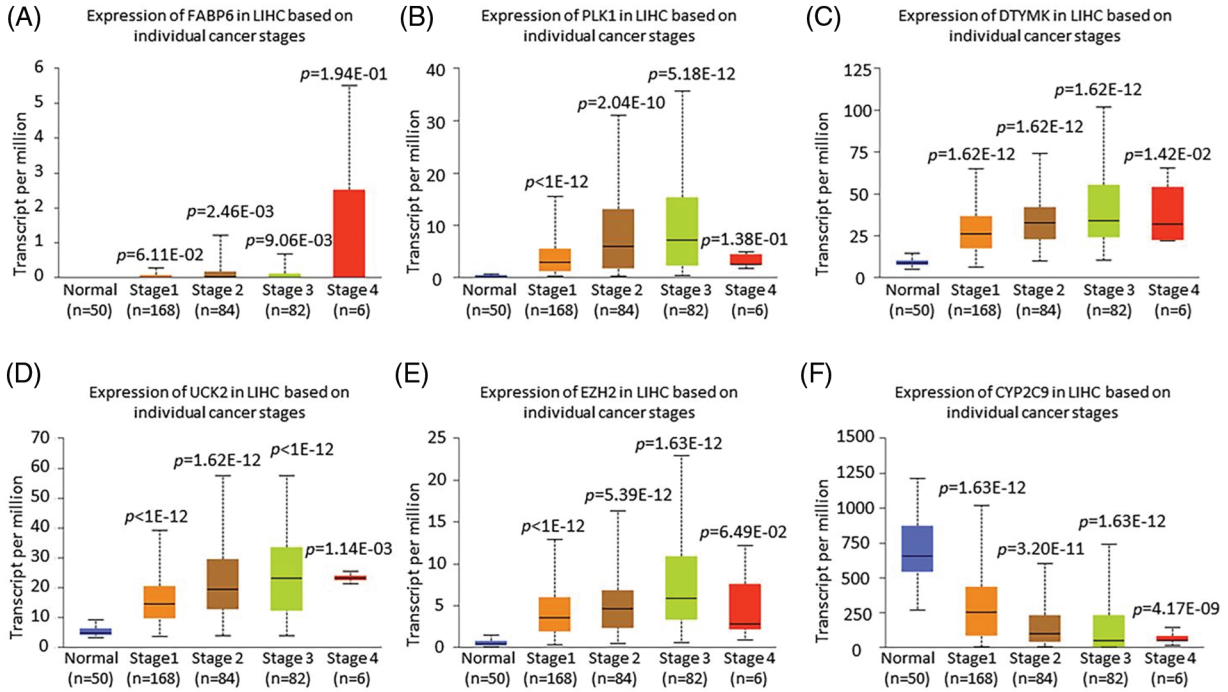

FIGURE 9. The expression of the 6 prognostic genes based on the stage using UALCAN. Differential expression of FABP6 (A), PLK1 (B), DTYMK (C), UCK2 (D), EZH2 (E), and CYP2C9 (F) based on the individual cancer stage.

to confer resistance to chemotherapy and radiation, making it a potential therapeutic target in liver cancer. Hence, the mRNA levels of UCK2 were validated in HEPG2 cells by RT-PCR. Tanshinone IIA treatment at both the concentrations was observed to lower the level of UCK2. Fig. 10A depicts these results. Further, the tanshinone IIA treatment decreased the protein expression of UCK2 in HEPG2 cells, as demonstrated by Western blot analysis (Fig. 10B).

Discussion

In this study, we first searched for tanshinone IIA targets. TCGA database was then used to acquire mRNA expression profiles and clinical information. We report 105 tanshinone IIA target genes that overlap with DEGs of HCC. The gene signature was identified and modeled using univariate Cox regression analysis combined with the LASSO Cox regression model. Subsequently, a novel 6-gene signature

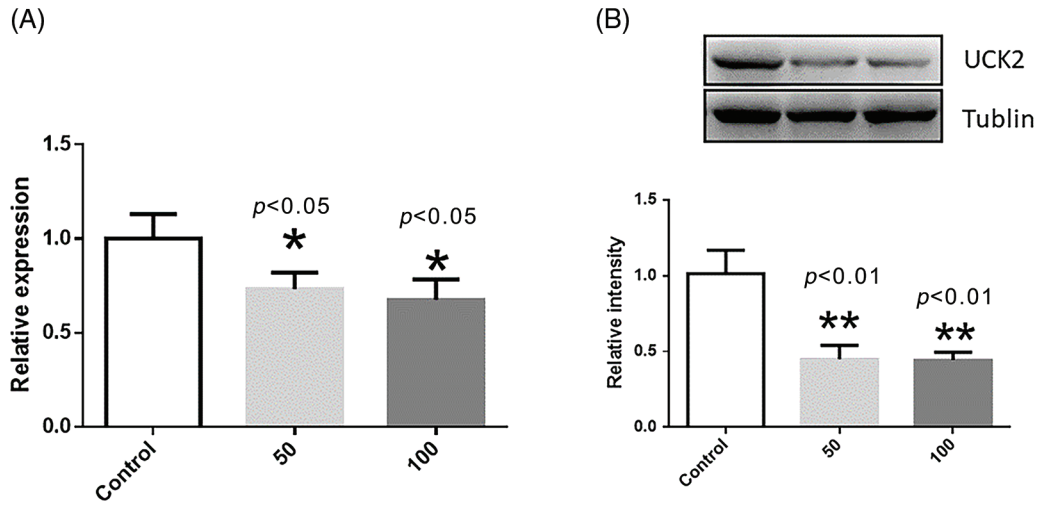

FIGURE 10. The mRNA level and protein expression of UCK2 after treatment with tanshinone IIA at different concentrations in HEPG2 cells. * represents $p < 0.05$, and ** represents $p < 0.01$. (A) The normalized mRNA level of UCK2 in the control (without tanshinone IIA), 50 and 100 μM of tanshinone IIA. (B) The normalized protein expression of UCK2 in the control (without tanshinone IIA), 50 and 100 μM tanshinone IIA.

(composed of FABP6, PLK1, DTYMK, UCK2, EZH2, and CYP2C9) was identified.

The risk score computed from the prognostic signature showed a significant impact on predicting the overall survival of a cancer patient. To elaborate, the high-risk patients had a poor prognosis. Subsequently, the nomogram based on the TNM stage and risk score was modeled to enhance this clinical diagnosis estimation. We discovered that the 6-gene signature was strongly correlated with the immune infiltration after studying the immune microenvironment. We identified six genetic features that were strongly associated with immune infiltration. Particularly, T cell and macrophage infiltration were highly related to the expression of the 6-gene signature.

Furthermore, the expression of the 6 genes was validated based on sample types and individual cancer stages. The results suggested that the novel 6-gene signature associated with immune infiltration can be a favorable potential biomarker. Meanwhile, the 6 genes are also the target genes of tanshinone IIA. Therefore, these 6 genes can be considered as anti-HCC therapeutic targets of tanshinone IIA. The mRNA and expression level of UCK2 were then confirmed by tanshinone IIA treatment in HEPG2 cells in the subsequent experiments.

As a machine learning algorithm, LASSO COX regression has been employed extensively in many studies (Liu *et al.*, 2019a, Wang *et al.*, 2020). The Cox proportional hazards regression model is the most commonly employed statistical model for survival analysis. Other traditional machine learning models, such as the Bayesian network, random forest, or artificial neural networks lack specific modules of survival analysis (Desai *et al.*, 2020). This study utilized the LASSO Cox regression model to discover and build the reported prognostic gene signature. The LASSO COX algorithm was shown to identify potential risk factors and evaluate the prediction and goodness of fit and clinical outcomes (Kantidakis *et al.*, 2020). The advantage of the LASSO COX algorithm model is that it can directly explain the relationship between risk factors and survival. Machine learning techniques are assumption-free and data-adaptive, which means they can be used effectively to model complex data. However, the LASSO COX algorithm also has some limitations. For example, the algorithm requires proper processing of input data and appropriate adjustment of parameters to avoid performance degradation (Scott *et al.*, 2019). Yet, to date, little focus has been given to the aspect of immune-infiltration and signature genes. Our study obtained a 6 gene signature and a nomogram that combined LASSO Cox regression and SVM-based deconvolution algorithm effectively improved the prognosis prediction of HCC.

To corroborate the precision of the results, the LASSO COX algorithm was implemented to solve the risk of over-fitting the prediction model derived from the high-dimensional data of liver cancer and to build prognostic characteristics. The multivariate COX regression was applied to create a nomogram based on the risk score and related clinical features. Risk scores and prognostic signatures demonstrated the potential advantages of survival prediction. After identifying the characteristics of 6 genes, the prognostic models of 6 genes were constructed and their prognostic abilities were studied. In the training and validation groups, the high- and low-risk patients had significantly different outcomes. All high-risk patients had a lower OS than low-risk patients. A time-dependent ROC analysis revealed that the 6 gene signature was significantly predictive.

The progression of a tumor is not only affected by the characteristics of the tumor itself, but also by the tumor microenvironment (Hinshaw and Shevde, 2019; Anderson and Simon, 2020). It should be noted that prognostic genes in this study were highly correlated to immune infiltration in the tumor microenvironment. According to CIBERSORTx analysis, resting memory CD4 T cells, resting NK cells, and activated mast cells exhibited significant variations in the high- and low-risk groups. Hence, the

findings of this research could pave the way for better treatment of HCC patients.

In conclusion, a novel 6-gene signature associated with tanshinone IIA drug targets was constructed and validated using the COX regression and LASSO regression algorithms *in vitro* experiments, and in prognostic analyses. The results showed that 6-gene signature associated with immune infiltration significantly improved the prediction outcomes in HCC patients. Therefore, the 6 gene signatures and nomograms proposed in this study have the potential to serve as predictive tools for HCC patients.

Funding Statement: This study was funded by the Sichuan Natural Science Foundation (No. 2022NSFSCO654); the Radiation Oncology Key Laboratory of Sichuan Province Open Fund (No. 2020FSZLX-03); and the UESTC-Sichuan Cancer Hospital 2021 Medical-Engineering Oncology Innovation Fund (No. ZYGX2021YGCX013).

Author Contributions: The authors confirm their contribution to the paper as follows: YG contributed to the conception and design of the study, and PW prepared the manuscript. GY analyzed the data and prepared some figures. All authors reviewed and approved the manuscript.

Availability of Data and Materials: The datasets generated during and/or analysed during the current study are available from the corresponding author on reasonable request.

Ethics Approval: Not applicable.

Conflicts of Interest: The authors declare that they have no conflicts of interest to report regarding the present study.

References

Allemann P, Demartines N, Bouzourene H, Tempia A, Halkic N (2013). Long-term outcome after liver resection for hepatocellular carcinoma larger than 10 cm. *World Journal of Surgery* **37**: 452–458. https://doi.org/10.1007/s00268-012-1840-5

Anderson NM, Simon MC (2020). The tumor microenvironment. *Current Biology* **30**: R921–R925. https://doi.org/10.1016/j.cub.2020.06.081

Balogh J, Victor D III, Asham EH, Burroughs SG, Boktour M, Saharia A, Li X, Ghobrial RM, Monsour HP Jr (2016). Hepatocellular carcinoma: A review. *Journal of Hepatocellular Carcinoma* **3**: 41–53. https://doi.org/10.2147/JHC.S61146

Batey RG, Burns T, Benson RJ, Byth K (1992). Alcohol consumption and the risk of cirrhosis. *The Medical Journal of Australia* **156**: 413–416. https://doi.org/10.5694/j.1326-5377.1992.tb139846.x

Bertot LC, Sato M, Tateishi R, Yoshida H, Koike K (2011). Mortality and complication rates of percutaneous ablative techniques for the treatment of liver tumors: A systematic review. *European Radiology* **21**: 2584–2596. https://doi.org/10.1007/s00330-011-2222-3

Bruix J, Raoul JL, Sherman M, Mazzaferro V, Bolondi L et al. (2012). Efficacy and safety of sorafenib in patients with advanced hepatocellular carcinoma: Subanalyses of a phase III trial. *Journal of Hepatology* **57**: 821–829. https://doi.org/10.1016/j.jhep.2012.06.014

Calle EE, Rodriguez C, Walker-Thurmond K, Thun MJ (2003). Overweight, obesity, and mortality from cancer in a prospectively studied cohort of U.S. adults. *The New England Journal of Medicine* **348**: 1625–1638. https://doi.org/10.1056/NEJMoa021423

Choo QL, Richman KH, Han JH, Berger K, Lee C et al. (1991). Genetic organization and diversity of the hepatitis C virus. *Proceedings of the National Academy of Sciences of the United States of America* **88**: 2451–2455. https://doi.org/10.1073/pnas.88.6.2451

Crissien AM, Frenette C (2014). Current management of hepatocellular carcinoma. *Gastroenterology & Hepatology* **10**: 153–161.

Desai RJ, Wang SV, Vaduganathan M, Evers T, Schneeweiss S (2020). Comparison of machine learning methods with traditional models for use of administrative claims with electronic medical records to predict heart failure outcomes. *JAMA Network Open* **3**: e1918962. https://doi.org/10.1001/jamanetworkopen.2019.18962

Deugnier Y, Turlin B (2001). Iron and hepatocellular carcinoma. *Journal of Gastroenterology and Hepatology* **16**: 491–494. https://doi.org/10.1046/j.1440-1746.2001.02430.x

Dyson J, Jaques B, Chattopadyhay D, Lochan R, Graham J et al. (2014). Hepatocellular cancer: The impact of obesity, type 2 diabetes and a multidisciplinary team. *Journal of Hepatology* **60**: 110–117. https://doi.org/10.1016/j.jhep.2013.08.011

El-Serag HB (2011). Hepatocellular carcinoma. *The New England Journal of Medicine* **365**: 1118–1127. https://doi.org/10.1056/NEJMra1001683

Fang ZY, Zhang M, Liu JN, Zhao X, Zhang YQ, Fang L (2021). Tanshinone IIA: A review of its anticancer effects. *Frontiers in Pharmacology* **11**: 611087. https://doi.org/10.3389/fphar.2020.611087

Fu Y, Wei XD, Guo L, Wu K, Le J, Ma Y, Kong X, Tong Y, Wu H (2022). The metabolic and non-metabolic roles of UCK2 in tumor progression. *Frontiers in Oncology* **12**: 904887. https://doi.org/10.3389/fonc.2022.904887

Gandini S, Botteri E, Iodice S, Boniol M, Lowenfels AB, Maisonneuve P, Boyle P (2008). Tobacco smoking and cancer: A meta-analysis. *International Journal of Cancer* **122**: 155–164. https://doi.org/10.1002/(ISSN)1097-0215

Gao C, Fang L, Zhao HC, Li JT, Yao SK (2013). Potential role of diabetes mellitus in the progression of cirrhosis to hepatocellular carcinoma: A cross-sectional case-control study from Chinese patients with HBV infection. *Hepatobiliary & Pancreatic Diseases International* **12**: 385–393. https://doi.org/10.1016/S1499-3872(13)60060-0

Gao J, Yang G, Pi R, Li R, Wang P, Zhang H, Le K, Chen S, Liu P (2008). Tanshinone IIA protects neonatal rat cardiomyocytes from adriamycin-induced apoptosis. *Translational Research: The Journal of Laboratory and Clinical Medicine* **151**: 79–87. https://doi.org/10.1016/j.trsl.2007.11.005

Green MR, Sambrook J (2018). Quantification of RNA by real-time reverse transcription-polymerase chain reaction (RT-PCR). *Cold Spring Harbor Protocols* **2018**. https://doi.org/10.1101/pdb.prot095042

Hao DC, Ge GB, Xiao PG (2018). Anticancer drug targets of salvia phytometabolites: Chemistry, biology and omics. *Current Drug Targets* **19**: 1–20. https://doi.org/10.2174/1389450117666161207141020

Hinshaw DC, Shevde LA (2019). The tumor microenvironment innately modulates cancer progression. *Cancer Research* **79**: 4557–4566. https://doi.org/10.1158/0008-5472.CAN-18-3962

Huang SY, Chang SF, Liao KF, Chiu SC (2017). Tanshinone IIA inhibits epithelial-mesenchymal transition in bladder cancer cells via modulation of STAT3-CCL2 signaling. *International Journal of Molecular Sciences* **18**: 1616. https://doi.org/10.3390/ijms18081616

Jieensinue S, Zhu H, Li G, Dong K, Liang M, Li Y (2018). Tanshinone IIA reduces SW837 colorectal cancer cell viability via the promotion of mitochondrial fission by activating JNK-Mff signaling pathways. *BMC Cell Biology* **19**: 21. https://doi.org/10.1186/s12860-018-0174-z

Kantidakis G, Putter H, Lancia C, Boer J, Braat AE, Fiocco M (2020). Survival prediction models since liver transplantation—comparisons between Cox models and machine learning techniques. *BMC Medical Research Methodology* **20**: 277. https://doi.org/10.1186/s12874-020-01153-1

Kanwal F, Kramer JR, Duan Z, Yu X, White D, El-Serag HB (2016). Trends in the burden of nonalcoholic fatty liver disease in a United States cohort of veterans. *Clinical Gastroenterology and Hepatology* **14**: 301-8.e1-2. https://doi.org/10.1016/j.cgh.2015.08.010

Larsson SC, Wolk A (2007). Overweight, obesity and risk of liver cancer: A meta-analysis of cohort studies. *British Journal of Cancer* **97**: 1005–1008. https://doi.org/10.1038/sj.bjc.6603932

Lee HP, Liu YC, Chen PC, Tai HC, Li TM et al. (2017). Tanshinone IIA inhibits angiogenesis in human endothelial progenitor cells *in vitro* and *in vivo*. *Oncotarget* **8**: 109217–109227. https://doi.org/10.18632/oncotarget.22649

Lee YJ, Lee JM, Lee JS, Lee HY, Park BH, Kim YH, Han JK, Choi BI (2015). Hepatocellular carcinoma: Diagnostic performance of multidetector CT and MR imaging–a systematic review and meta-analysis. *Radiology* **275**: 97–109. https://doi.org/10.1148/radiol.14140690

Lencioni R, Cioni D, Crocetti L, Franchini C, Pina CD, Lera J, Bartolozzi C (2005). Early-stage hepatocellular carcinoma in patients with cirrhosis: Long-term results of percutaneous image-guided radiofrequency ablation. *Radiology* **234**: 961–967. https://doi.org/10.1148/radiol.2343040350

Li YI, Elmer G, Leboeuf RC (2008). Tanshinone IIA reduces macrophage death induced by hydrogen peroxide by upregulating glutathione peroxidase. *Life Sciences* **83**: 557–562. https://doi.org/10.1016/j.lfs.2008.08.003

Liao XZ, Gao Y, Huang S, Chen ZZ, Sun LL, Liu JH, Chen HR, Yu L, Zhang JX, Lin LZ (2019). Tanshinone IIA combined with cisplatin synergistically inhibits non-small-cell lung cancer *in vitro* and *in vivo* via down-regulating the phosphatidylinositol 3-kinase/Akt signalling pathway. *Phytotherapy Research* **33**: 2298–2309. https://doi.org/10.1002/ptr.6392

Liu Z, Li M, Hua Q, Li Y, Wang G (2019a). Identification of an eight-lncRNA prognostic model for breast cancer using WGCNA network analysis and a Cox proportional hazards model based on L1-penalized estimation. *International Journal of Molecular Medicine* **44**: 1333–1343. https://doi.org/10.3892/ijmm.2019.4303

Liu Z, Zhu W, Kong X, Chen X, Sun X, Zhang W, Zhang R (2019b). Tanshinone IIA inhibits glucose metabolism leading to apoptosis in cervical cancer. *Oncology Reports* **42**: 1893–1903. https://doi.org/10.3892/or.2019.7294

Llovet JM, Ricci S, Mazzaferro V, Hilgard P, Gane E et al. (2008). Sorafenib in advanced hepatocellular carcinoma. *The New England Journal of Medicine* **359**: 378–390. https://doi.org/10.1056/NEJMoa0708857

Llovet JM, Zucman-Rossi J, Pikarsky E, Sangro B, Schwartz M, Sherman M, Gores G (2016). Hepatocellular carcinoma. *Nature Reviews Disease Primers* **2**: 16018. https://doi.org/10.1038/nrdp.2016.18

Ma L, Jiang H, Xu X, Zhang C, Niu Y et al. (2019). Tanshinone IIA mediates SMAD7-YAP interaction to inhibit liver cancer growth by inactivating the transforming growth factor beta signaling pathway. *Aging* **11**: 9719–9737. https://doi.org/10.18632/aging.102420

Mazzaferro V, Regalia E, Doci R, Andreola S, Pulvirenti A, Bozzetti F, Montalto F, Ammatuna M, Morabito A, Gennari L (1996). Liver transplantation for the treatment of small hepatocellular carcinomas in patients with cirrhosis. *The New England Journal of Medicine* **334**: 693–699. https://doi.org/10.1056/NEJM199603143341104

Newman AM, Steen CB, Liu CL, Gentles AJ, Chaudhuri AA et al. (2019). Determining cell type abundance and expression from bulk tissues with digital cytometry. *Nature Biotechnology* **37**: 773–782. https://doi.org/10.1038/s41587-019-0114-2

Nolan T, Hands RE, Bustin SA (2006). Quantification of mRNA using real-time RT-PCR. *Nature Protocols* **1**: 1559–1582. https://doi.org/10.1038/nprot.2006.236

Ott JJ, Stevens GA, Groeger J, Wiersma ST (2012). Global epidemiology of hepatitis B virus infection: New estimates of age-specific HBsAg seroprevalence and endemicity. *Vaccine* **30**: 2212–2219. https://doi.org/10.1016/j.vaccine.2011.12.116

Reddy JK, Rao MS (2006). Lipid metabolism and liver inflammation. II. Fatty liver disease and fatty acid oxidation. *American Journal of Physiology-Gastrointestinal and Liver Physiology* **290**: G852–G858. https://doi.org/10.1152/ajpgi.00521.2005

Ren X, Wang C, Xie B, Hu L, Chai H, Ding L, Tang L, Xia Y, Dou X (2017). Tanshinone IIA induced cell death via miR30b-p53-PTPN11/SHP2 signaling pathway in human hepatocellular carcinoma cells. *European Journal of Pharmacology* **796**: 233–241. https://doi.org/10.1016/j.ejphar.2016.11.046

Sangiovanni A, Manini MA, Iavarone M, Romeo R, Forzenigo LV et al. (2010). The diagnostic and economic impact of contrast imaging techniques in the diagnosis of small hepatocellular carcinoma in cirrhosis. *Gut* **59**: 638–644. https://doi.org/10.1136/gut.2009.187286

Sangro B, Carpanese L, Cianni R, Golfieri R, Gasparini D et al. (2011). Survival after yttrium-90 resin microsphere radioembolization of hepatocellular carcinoma across Barcelona clinic liver cancer stages: A European evaluation. *Hepatology* **54**: 868–878. https://doi.org/10.1002/hep.24451

Scott IA, Cook D, Coiera EW, Richards B (2019). Machine learning in clinical practice: Prospects and pitfalls. *The Medical Journal of Australia* **211**: 203–205.e1. https://doi.org/10.5694/mja2.50294

Steen CB, Liu CL, Alizadeh AA, Newman AM (2020). Profiling cell type abundance and expression in bulk tissues with CIBERSORTx. *Methods in Molecular Biology* **2117**: 135–157. https://doi.org/10.1007/978-1-0716-0301-7

Su CC (2018). Tanshinone IIA can inhibit MiaPaCa2 human pancreatic cancer cells by dual blockade of the Ras/Raf/MEK/ERK and PI3K/AKT/mTOR pathways. *Oncology Reports* **40**: 3102–3111. https://doi.org/10.3892/or.2018.6670

Takayasu K, Arii S, Ikai I, Omata M, Omata K et al. (2006). Prospective cohort study of transarterial chemoembolization for unresectable hepatocellular carcinoma in 8510 patients. *Gastroenterology* **131**: 461–469. https://doi.org/10.1053/j.gastro.2006.05.021

Torre LA, Bray F, Siegel RL, Ferlay J, Lortet-Tieulent J, Jemal A (2015). Global cancer statistics, 2012. *CA: A Cancer Journal for Clinicians* **65**: 87–108. https://doi.org/10.3322/caac.21262

Verslype C, Rosmorduc O, Rougier P, ESMO Guidelines Working Group. (2012). Hepatocellular carcinoma: ESMO-ESDO clinical practice guidelines for diagnosis, treatment and follow-up. *Annals of Oncology* **23**: vii41–vii48. https://doi.org/10.1093/annonc/mds225

Villanueva A (2019). Hepatocellular carcinoma. *The New England Journal of Medicine* **380**: 1450–1462. https://doi.org/10.1056/NEJMra1713263

Wang C, Wang X, Gong G, Ben Q, Qiu W, Chen Y, Li G, Wang L (2012). Increased risk of hepatocellular carcinoma in patients with diabetes mellitus: A systematic review and meta-analysis of cohort studies. *International Journal of Cancer* **130**: 1639–1648. https://doi.org/10.1002/ijc.26165

Wang Z, Zhu J, Liu Y, Liu C, Wang W, Chen F, Ma L (2020). Development and validation of a novel immune-related prognostic model in hepatocellular carcinoma. *Journal of Translational Medicine* **18**: 67. https://doi.org/10.1186/s12967-020-02255-6

White DL, Tavakoli-Tabasi S, Kuzniarek J, Pascua R, Ramsey DJ, El-Serag HB (2012). Higher serum testosterone is associated with increased risk of advanced hepatitis C-related liver disease in males. *Hepatology* **55**: 759–768. https://doi.org/10.1002/hep.24618

Yin X, Yin Y, Cao FL, Chen YF, Peng Y, Hou WG, Sun SK, Luo ZJ (2012). Tanshinone IIA attenuates the inflammatory response and apoptosis after traumatic injury of the spinal cord in adult rats. *PLoS One* **7**: e38381. https://doi.org/10.1371/journal.pone.0038381

Yuan JM, Ross RK, Stanczyk FZ, Govindarajan S, Gao YT, Henderson BE, Yu MC (1995). A cohort study of serum testosterone and hepatocellular carcinoma in Shanghai, China. *International Journal of Cancer* **63**: 491–493. https://doi.org/10.1002/(ISSN)1097-0215

Zhang X, Zhou Y, Gu YE (2019). Tanshinone IIA induces apoptosis of ovarian cancer cells *in vitro* and *in vivo* through attenuation of PI3K/AKT/JNK signaling pathways. *Oncology Letters* **17**: 1896–1902. https://doi.org/10.3892/ol.2018.9744

Zhang Y, Guo S, Fang J, Peng B, Zhang Y, Cao T (2018). Tanshinone IIA inhibits cell proliferation and tumor growth by downregulating STAT3 in human gastric cancer. *Experimental and Therapeutic Medicine* **16**: 2931–2937. https://doi.org/10.3892/etm.2018.6562

Zhao D, Tong L, Zhang L, Li H, Wan Y, Zhang T (2016). Tanshinone IIA stabilizes vulnerable plaques by suppressing RAGE signaling and NF-κB activation in apolipoprotein-E-deficient mice. *Molecular Medicine Reports* **14**: 4983–4990. https://doi.org/10.3892/mmr.2016.5916

Supplementary Materials

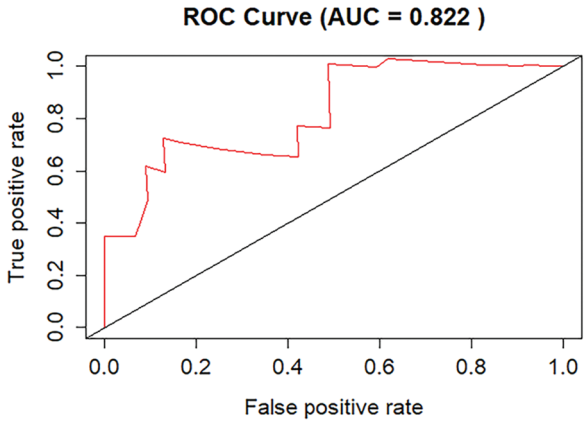

FIGURE S1. The mean area under the curve (AUC) values of the 5-fold cross-validation.

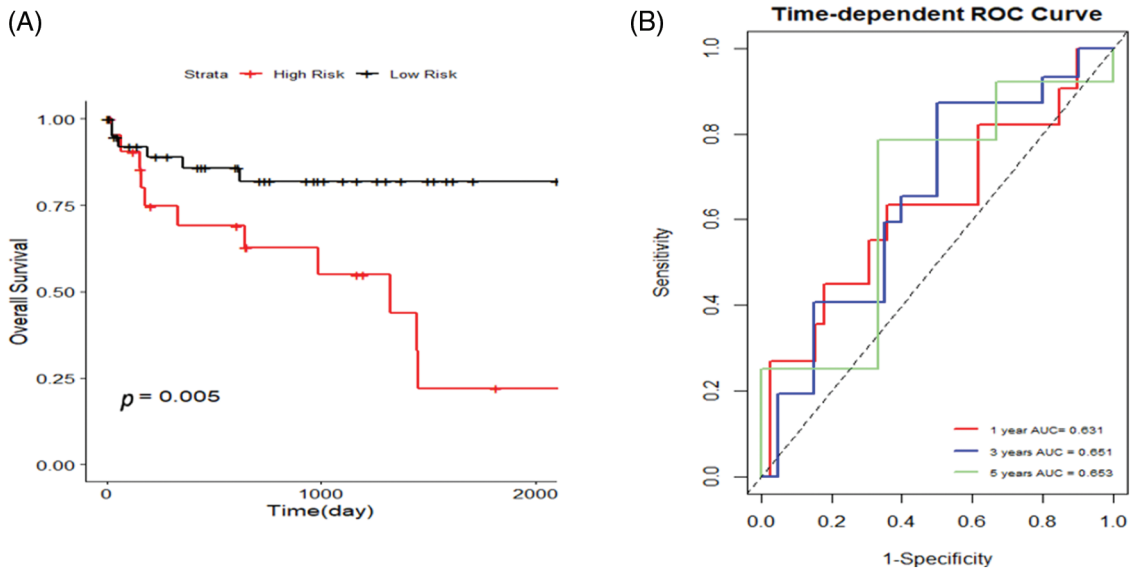

FIGURE S2. The Gene Expression Omnibus (GEO) dataset GSE76427 was additionally searched for validation, and K-M curves and 1, 3, and 5-year area under the curve (AUC) curves were plotted to validate the risk model.

TABLE S1

A list of the 286 targets of tanshinone IIA

No.	Target genes
1	ACHE
2	ADRA1D
3	ADRB2
4	AHSA1
5	BCL2
6	CALCR
7	CASP3
8	CDKN1A
9	CHRM1
10	CHRM2
11	CHRM3
12	CHRM4
13	CHRM5
14	CYP1A1
15	CYP1A2
16	CYP3A4
17	DPP4
18	DRD1
19	ECE1
20	EDN1
21	EDNRA
22	FASN
23	FOS
24	ITGB3
25	JUN
26	MMP9
27	MYC
28	NCOA1
29	NFKBIA
30	NPM1
31	NR1I2
32	OPRD1
33	OPRM1
34	PARP4
35	PTGS2
36	RELA
37	RXRA
38	TP53
39	ABL1
40	ABO
41	ACE
42	ADAM17
43	ADAM33
44	ADH1C
45	ADH5
46	ADK
47	AKR1B1
48	AKR1C1
49	AKR1C2
50	AKR1C3
51	AKT1
52	AKT2
53	ALB
54	AMD1

(Continued)

Table S1 (continued)

(Continued)

Table S1 (continued)

No.	Target genes
55	AMY1A
56	ANG
57	ANXA5
58	AR
59	ARG1
60	ATIC
61	AURKA
62	BACE1
63	BCAT2
64	BCHE
65	BCL2L1
66	BHMT
67	BIRC7
68	BLVRB
69	BMP2
70	BRAF
71	BTK
72	CA2
73	CALM1
74	CASP1
75	CBR1
76	CBS
77	CCNA2
78	CCNT1
79	CDK2
80	CDK5
81	CDK5R1
82	CDK6
83	CDK9
84	CES1
85	CFB
86	CFD
87	CHEK1
88	CRABP2
89	CTNNA1
90	CTSB
91	CTSF
92	CTSK
93	CTSS
94	CYP2C8
95	CYP2C9
96	DAPK1
97	DCK
98	DHFR
99	DHODH
100	DPEP1
101	DTYMK

(Continued)

Table S1 (continued)

No.	Target genes
102	DUSP6
103	DUT
104	EGFR
105	EIF4E
106	ELANE
107	EPHB4
108	EPHX2
109	ERBB4
110	ERI1
111	ESR1
112	ESRRA
113	ESRRG
114	F10
115	F11
116	F2
117	F7
118	FABP3
119	FABP4
120	FABP6
121	FABP7
122	FDPS
123	FECH
124	FGFR1
125	FGFR2
126	FGG
127	FKBP1A
128	FKBP3
129	FNTA
130	FNTB
131	FOLH1
132	GART
133	GC
134	GCK
135	GLO1
136	GM2A
137	GPI
138	GRB14
139	GRB2
140	GSK3B
141	GSR
142	GSTA1
143	GSTA3
144	GSTM1
145	GSTM2
146	GSTP1
147	GSTT2B
148	HADH

(Continued)

Table S1 (continued)

No.	Target genes
149	HCK
150	HDAC8
151	HMGCR
152	HMOX1
153	HNF4G
154	HNMT
155	HPGDS
156	HSD11B1
157	HSD17B1
158	HSP90AA1
159	HSP90AB1
160	IGF1
161	IGF1R
162	IL2
163	IMPDH2
164	INSR
165	ITGAL
166	ITK
167	IVD
168	JAK2
169	JAK3
170	KAT2B
171	KDR
172	KIF11
173	KIT
174	LCK
175	LCN2
176	LTA4H
177	MAOB
178	MAP2K1
179	MAPK1
180	MAPK10
181	MAPK14
182	MAPK8
183	MAPKAPK2
184	MDM2
185	MET
186	METAP2
187	MIF
188	MME
189	MMP12
190	MMP13
191	MMP2
192	MMP3
193	MMP7
194	MMP8
195	MTAP

(Continued)

Table S1 (continued)

No.	Target genes
196	MTHFD1
197	NCOA2
198	NCOA5
199	NOS3
200	NQO1
201	NQO2
202	NR1H2
203	NR1H3
204	NR1H4
205	NR1I3
206	NR3C1
207	NR3C2
208	NT5M
209	OAT
210	PADI4
211	PAK5
212	PARP1
213	PCK1
214	PCTP
215	PDE3B
216	PDE4B
217	PDE4D
218	PDE5A
219	PDK2
220	PDPK1
221	PGF
222	PGR
223	PIK3CG
224	PIK3R1
225	PIM1
226	PITPNA
227	PKIA
228	PLA2G2A
229	PLK1
230	PNMT
231	PPARA
232	PPARD
233	PPARG
234	PPIA
235	PPP1CC
236	PPP5C
237	PRKCQ
238	PROCR
239	PSAP
240	PTPN1
241	PTPN11
242	PYGL

(Continued)

Table S1 (continued)

No.	Target genes
243	RAB5A
244	RAP2A
245	RARA
246	RARB
247	RARG
248	RBP4
249	REN
250	RFK
251	RORA
252	RXRB
253	SDS
254	SEC14L2
255	SERPINA1
256	SETD7
257	SHBG
258	SHMT1
259	SIRT5
260	SOD2
261	SORD
262	SRC
263	STS
264	SULT1E1
265	SULT2A1
266	SULT2B1
267	SYK
268	TEK
269	TGFB2
270	TGFBR1
271	TGM3
272	THRA
273	THRB
274	TNNC1
275	TPH1
276	TPSB2
277	TRAPPC3
278	TRDMT1
279	TTPA
280	TTR
281	TYMS
282	UCK2
283	VDR
284	WAS
285	XIAP
286	ZAP70